Applied Energy 185 (2017) 1173–1184

Contents lists available at ScienceDirect

Applied Energy

journal homepage: www.elsevier.com/locate/apenergy

Optimal control of a wind–PV-hybrid powered heat pump water heater ☆

Sam Sichilalu *, Tebello Mathaba, Xiaohua Xia

Centre of New Energy Systems, Department of Electrical, Electronic and Computer Engineering, University of Pretoria, Pretoria 0002, South Africa

HIGHLIGHTS

- Optimal control of a wind–PV-hybrid powered heat pump water heater is modelled.
- Daily energy cost saving of around 70.74% is shown.
- Saved energy is due to proposed optima control intervention with time-of-use.
- Potential of a daily energy saving of about up to 51.23% is shown.
- The optimal photovoltaic and wind energy feed-into the grid is modelled.

ARTICLE INFO

Article history:
Received 3 July 2015
Received in revised form 8 October 2015
Accepted 9 October 2015
Available online 12 November 2015

Keywords:
Heat pump water heater
Optimal switching control
Photovoltaic
Wind generator
Time-of-use tariff
Mixed integer linear program

ABSTRACT

This paper develops an optimal control (OC) model of a heat pump water heater (HPWH) supplied by a wind generator–photovoltaic-grid system. The objective function is energy cost minimization, taking into account the time-of-use electricity tariff, which is an important control parameter. The control variables are the supply switch to the HPWH and the power from the grid, while the hot water temperature inside the tank is the state variable. The model meets both the HPWH's technical and operational constraints in providing hot water at a desired temperature and achieves load shifting. This problem is solved using a mixed integer linear program. The results show a 70.7% cost reduction upon implementation of this intervention. A case study is done and the OC shows significant potential in both energy and cost saving in comparison to the digital thermostat controller used in most of the HPWHs on the market. The economic analysis is presented in this paper as well.

1. Introduction

The energy consumption in buildings account for about 42% of global energy production, especially in developed countries [1]; 60.51% of this energy goes for space heating while 23.60% goes for water heating at domestic[1] level. Therefore, in order to reduce the high energy consumption, energy-efficient equipment, such as heat pump water heaters (HPWH), needs to be employed for demand side management (DSM) at domestic level. HPWHs are devices that drive heat energy from a cooler surrounding medium to a much warmer place using a working fluid (refrigerant). The refrigerant absorbs the ambient energy of the surrounding medium in the evaporator and passes through the compressor, where it gains extra heat energy through an increase in pressure as a result of compression. This hot working fluid then circulates through the heat exchanger (condenser), where thermal energy is transferred to the water and the process is repeated. The past two decades have seen major advances in HPWH technology [2–4], which has led to its wider application and improved coefficient of performance (COP). Essen and Yuksel [5] extensively investigated both ground-sourced and air-sourced HPWHs and made an economic analysis. Various authors [6–11] have developed models and investigated ways of improving the COP of the HPWH; however, most of them agree that optimal control (OC), system design, sizing and integration remain technological challenges.

The problem of DSM requires a multi-directional approach; the HPWHs alone might not achieve significant energy savings, hence the need to integrate them with distributed renewable energy sources (DREs) such as wind and photovoltaic (PV) power in buildings [12,13]. On/off-site DRE integration into buildings and small communities is a promising technology for DSM. Various hybrid DREs are presented in [14–20], though much of the success achieved so far is in the sizing and system design. More effort

☆ This paper was presented at the 7th International Conference on Applied Energy (ICAE2015), March 28–31, 2015, Abu Dhabi, UAE (Original paper title: "Optimal power control of grid tied PV-battery-diesel system powering heat pump water heaters" and Paper No.: 66).

* Corresponding author. Tel.: +27 12 420 6767; fax: +27 12 362 5000.
E-mail addresses: Sam.Sichilalu@up.ac.za, sichgroup@yahoo.com (S. Sichilalu).

[1] http://www.dti.gov.uk/energy/inform/.

http://dx.doi.org/10.1016/j.apenergy.2015.10.072
0306-2619/

Nomenclature

$P_w(t)$	wind generator power output (kW)
$P_{pv}(t)$	photovoltaic power output (kW)
$P_g(t)$	grid power (kW)
P_{hp}	heat pump water heater power demand (kW)
COP	coefficient of performance
$u(t)$	heat pump power supply switch control variable (0 or 1)
$T(t)$	hot water temperature inside the tank (°C)
T_{low} and T_{up}	lower and upper hot water temperature set points (°C)
T_a	ambient temperature (°C)
T_o	initial hot water temperature (°C)
$T_{in}(t)$	inlet cold water temperature (°C)
R	South African rands (1R = 0.074 USD as of 22.09.2015)
$p(t)$	time-of-use electricity price (R/kW h)
N	total number of sampling intervals
t_s and k	sampling time (h) and kth sampling interval respectively
J	cost function
Q_D	total losses due to water demand
Q_L	total standby (convectional) losses
$W_D(t)$	flow rate (l/h)
q_{loss}	conventional loss in (W/m^2)
Δx	thickness of the insulation (m)
h	surface heat transfer coefficient (W/m^{2}K)
κ	thermal conductivity (W/m K)
S_{area}	total surface area (m^2)
c	specific heat capacity of water (J/kg °C)
ø	diameter (m)
$\dot{T}$	derivative of temperature
L	mass of water inside the tank (kg)
η_t	turbine coupling gearbox efficiency (%)
η_g	wind generator efficiency (%)
ρ	air density factor of the wind generator
C_p	Betz limit
A_w	wind generator rotor sweeping area (m^2)
V_N	rated wind speed (m/s)
V_r	wind speed (m/s)
P_{wr}	rated wind turbine power output (kW)
V_i	cut-in wind speed (m/s)
V_c	cut-off wind speed (m/s)
NPV	net present value
PV	present value
m	project life period (years)
r	interest rate or discount rate
n	time in years before the future cash flow occurs
MILP	mixed integer linear program
TOU	time-of-use electricity tariff
Eskom	South African power utility company

and research are required to integrate these DREs optimally into energy-efficient household loads (e.g. heat pumps) to realize net-zero energy buildings [21], cost-effective billing and positive-energy buildings [22]. Therefore, future optimal energy-mixing will rely on the successful implementation of OC techniques [23–25].

The main problem of digital thermostat control systems used in HPWHs and some tank hot water heaters (geysers) on the market, is the dependency of its operation on temperature set-points only and does not change its assumed operating state between the intervals. Digital thermostat actuation occurs upon hitting the lower/upper set-point, which prolongs the operation time and consumes lots of energy. This control system is unable to optimally control either demand prediction or load-shifting to avoid operation during peak time-of-use (TOU) electricity tariff periods, that could save energy and cost. Most geysers in South Africa are fitted with a thermostat control system actuating only every lapse of thermostat dead-band interval below the set-point, operating continuously even in periods when there is no demand for hot water. Moreover, this hot water generating equipment accounting for 23.60% energy consumption in the building is rarely integrated into DREs.

Therefore, this paper proposes a first attempt at optimal control system application in HPWHs that is superior to digital thermostat control limitations. A further novelty is in the successful optimal integration of the DREs, such as wind into the supply of heat pumps, which has not yet been explored in literature. This DRE-HPWH model meets both the technical and operational constraints, deals with excess energy feed-in and provides the desired hot water temperature optimally under the TOU tariff. In comparison to the digital thermostat control system, this paper's OC technology can effectively predict within the control horizon with known hot water demand, an optimal hot water temperature without necessarily reaching the set-points. This in turn minimizes the energy required to raise the water temperature till set-point. This model has the potential to achieve practical net-zero energy building with cost-effective consumption. An addition contribution is that unlike many previous works that evaluated the techno-economic benefit [26–32], i.e., the objective functions are performances over a year, or multiple years, this paper proposes operational performances that are evaluated over a much shorter period, such as a day, 24 h. A short period enables end-users to monitor their daily energy usage rather than accumulative annual totals effectively. The daily savings eventually accumulate into savings over weeks, months, seasons and years. The end-user effectively assesses and can understand energy consumption trends and its cost implications on a daily basis. This is a major difference in this paper.

This paper is structured as follows: Sections 2 and 3 present the mathematical model formulation and Section 4 the simulation results and discussion. The last part, Section 5, is the conclusion.

2. Mathematical model formulation

2.1. Schematic model layout

The optimal switching strategy schematic diagram of the heat pump shown in Fig. 1 comprises the wind generator $P_w(t)$, PV modules $P_{pv}(t)$, grid $P_g(t)$ and an air-sourced heat pump with tank-wrapped condenser $P_{hp}(t)$. The switch $u(t)$ controls the power supply to the HPWH. The excess renewable power is fed into the grid. The grid power $P_g(t)$ accepts power from renewable power sources as well as it supplements the heat pump whenever their combined output fails to meet the demand.

The TOU electricity tariff is one of the important control parameters in the optimal switching strategy of the HPWH, especially in the peak period. $T(t)$ is the state variable, viz the temperature of the water inside the storage tank. The hot water demand $W_D(t)$ is the flow rate in liters/hour taken from the case study. The desired hot water temperature is predetermined at between T_{low} and T_{up}, which are the lower and upper temperature set-point respectively. However, these limits may vary from one individual to another. The control variables in this paper are the grid power $P_g(t)$ and heat pump supply switch $u(t)$.

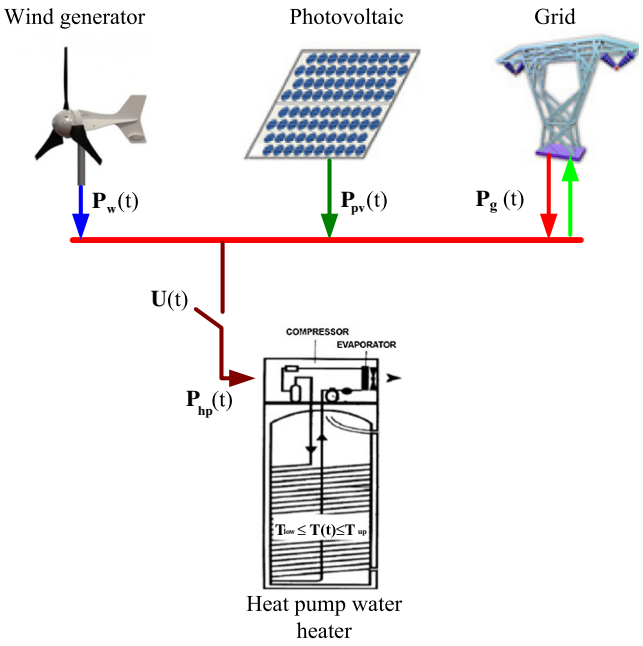

Fig. 1. Schematic layout of the model.

2.2. Sub-models

2.2.1. Heat pump water heater

The heat pump model is developed according to [33], with a fixed power demand P_{hp} rating, operating at full capacity. The temperature distribution of the hot water is assumed to be uniform in a constant water volume, neglecting stratification. For modeling simplicity, the energy losses in the evaporator, refrigerant and compressor are neglected; however, the efficiency of the electric motor driving the compressor is around 96%. The overall efficiency of other thermal components of the HPWH is accounted for by COP in the case study. In order to minimize the complexity of this modeling problem, a constant COP is assumed as well, though, practically it varies. Therefore, only energy losses due to hot water demand $Q_D(t)$ and convectional (standby) loss $Q_L(t)$ are modeled in this paper.

The standby losses, $Q_L(t)$, are thermal losses dispatched through the tank's casing material. These losses can be minimized through increased thermal insulation and application of low thermal conductivity materials. The per second convention loss q_{loss} in W/m^2, according to [34], is given in Eq. (1),

$$q_{loss}(T(t), T_a) = \frac{T(t) - T_a}{\frac{\Delta x}{\kappa} + \frac{1}{h}}, \tag{1}$$

where Δx and κ are the insulation thickness and thermal conductivity coefficients respectively, h is the surface heat transfer coefficient of the tank and $T(t), T_a$ are the hot water and ambient temperature respectively. Therefore, for a given tank surface area S_{area}, the total standby losses are:

$$Q_L(T(t), T_a) = q_{loss} S_{area}. \tag{2}$$

The other loss is associated with the hot water demand $Q_D(t)$, which triggers the inlet cold water into the tank to maintain a constant volume. Therefore, $T(t)$ drops during hot water demand period because of the inlet of cold water into the tank. Losses associated with the hot water demand are given as [35,36] in Eq. (3):

$$Q_D(t) = cW_D(t)(T(t) - T_{in}), \tag{3}$$

where $c = 4180$ J/kg/°C is the specific heat capacity of water. T_{in} is the municipal inlet water temperature whereas $W_D(t)$ is the hot water demand flow rate in liters/hour.

In order to satisfy the HPWH thermal output requirements, the corresponding electrical power input is [9,35]:

$$P_{hp}(t) = \frac{Q_D(t) + Q_L(t)}{COP}. \tag{4}$$

The power balance is a dynamic equation. Let $Q_H(t)$ be the total HPWH heat output kilowatts and L the water mass (tank capacity) in kilograms. Therefore, the power balance becomes a first derivative differential function given in Eq. (5) [37].

$$cL\dot{T}(t) = Q_H(t) - Q_L(t) - Q_D(t), \tag{5}$$

$$Q_H(t) = P_{hp} COPu(t). \tag{6}$$

By substituting Eq. (1)–(4) into Eq. (5), one gets

$$\dot{T}(t) = \frac{P_{hp} COPu(t) - S_{area}\left(\frac{T(t) - T_a}{\frac{\Delta x}{\kappa} + \frac{1}{h}}\right) - cW_D(t)(T(t) - T_{in}(t))}{cL}, \tag{7}$$

denoting:

$$\alpha(t) = \frac{S_{area}}{cL\left(\frac{\Delta x}{\kappa} + \frac{1}{h}\right)} + \frac{W_D(t)}{L}, \tag{8}$$

$$\beta = \frac{P_{hp} COP}{cL}, \tag{9}$$

$$\gamma(t) = \frac{S_{area} T_a}{cL\left(\frac{\Delta x}{\kappa} + \frac{1}{h}\right)} + \frac{W_D(t) T_{in}(t)}{L}, \tag{10}$$

then Eq. (7) becomes:

$$\dot{T}(t) = -\alpha(t)T(t) + \beta u(t) + \gamma(t). \tag{11}$$

2.2.2. Wind generator

In this study a simplified wind generator model is given in Eq. (12), according to [38]:

$$P_w(t) = \eta_t \eta_g 0.5 \rho_a C_p A_w V_r^3, \tag{12}$$

where η_t and η_g are the mechanical gearbox and generator efficiency respectively, ρ is the air density factor, C_p is the turbine power coefficient (Betz limit), A_w is the turbine rotor sweeping area and lastly, V_r is the wind speed.

The rated wind speed V_N is calculated as [39]

$$V_N = \sqrt[3]{\frac{P_{wr}}{\eta_t \eta_g 0.5 \rho_a C_p A_w}}, \tag{13}$$

where V_N and P_{wr} are the rated wind speed and power respectively. Though this is a simplified model, a typical turbine power output characteristic is proportional to cubed wind speed between the cut-in wind speed V_i and rated wind speed V_N at the maximum aerodynamic efficiency. Above V_N, the pitched blades reduce the aerodynamic efficiency, hence keeping the power output constant. If the speed exceeds the pitch control limit, it reaches a cut-out wind speed V_c, cutting the power production. The hub height of the turbine with annual mean wind speeds [18] between 6 and 8 m/s at 10 m height anemometer is calculated at approximately 1.2 times the rotor sweeping diameter [39]. The wind model parameters are from the case study given in Table 2. The excess wind power is fed into the grid using the established wind energy feed-in tariff.

2.2.3. Photovoltaic power

The PV power generation $P_{pv}(t)$ are input data in this model. A power source from zero to its maximum rated measured value is taken from the case study of our previous research [13,40]. The PV power input data are given in Fig. 5. The PV supplies $P_{pv}(t)$ to the HPWH and the excess is sold to the grid at the prevailing feed-in tariff. This model excludes the energy storage system in order to lower the initial investment cost, which hampers the implementation of these systems at household level. The grid acts as the DREs' energy storage system. The PV power generation is bounded by:

$$0 \leqslant P_{pv}(t) \leqslant P_{pv}^{max}. \tag{14}$$

2.2.4. Grid power

The grid is modeled as an infinite bar capable of simultaneously supplying and accepting power from the solar PV and wind generator. The TOU electricity tariff is one of the most important OC parameters. In South Africa, Eskom is the main power supply utility company and has both a flat and a dynamic TOU electricity tariff pricing $p(t)$ system. In this model the TOU electricity tariff is considered: off-peak (p_o), standard (p_s) and peak (p_p). The recent Eskom[2] megaflex active energy-TOU tariff is incorporated as a control parameter. The Eskom TOU electricity tariff is:

$$p(t) = \begin{cases} p_o = 0.3656\text{R/kW h} & \text{if } t \in [0,\ 7] \cup [23,\ 24], \\ p_s = 0.6733\text{R/kW h} & \text{if } t \in [7,\ 8] \cup [11,\ 19] \cup [21,\ 23], \\ p_p = 2.2225\text{R/kW h} & \text{if } t \in [8,\ 11] \cup [19,\ 21], \end{cases} \tag{15}$$

where R is the South African rand and t is the time of day with $t = 0, \ldots, 23$.

The grid can accept excess power from wind and PV and complement the renewable resources in meeting the heat pump load. However the feed-in and supply do not happen concurrently owing to the linearity nature of the grid power constraint. The power balance is written as:

$$P_{hp}u(t) - P_g(t) = P_w(t) + P_{pv}(t). \tag{16}$$

The DREs' feed-in tariff is regulated by the National Energy Regulator of South Africa (NERSA),[3] a regulatory to establish the renewable energy feed-in tariff for South Africa. NERSA, through the renewable energy purchasing agency in South Africa, is the single buyer office (SBO) of the national electricity utility, Eskom, under phase II (PV systems large ground or roof-mounted). These regulatory measures and SBO provide the necessary incentive to DRE developers and private investors. They guarantee the availability of a renewable energy market and provide venture capitalist at low financial risk. The prevailing PV feed-in tariff is 3.94 R/kW h, whereas for wind it is 1.25 R/kW h.

3. Discrete model formulation

3.1. Discretized hot water temperature

The water demand flow rate $W_D(t)$ and the inlet water, $T_{in}(t)$, are functions of time taken from the case study. The general discrete formulation of Eq. (11) in terms of the k-th hot water temperature is given in Eq. (17):

$$T_{k+1} = (1 - t_s\alpha_k)T_k + t_s\beta u_k + t_s\gamma_k. \tag{17}$$

Then, T_{k+1} at each interval can be derived as:

$$\begin{aligned} T_1 &= (1 - t_s\alpha_0)T_o + t_s\beta u_0 + t_s\gamma_0, \\ T_2 &= [(1 - t_s\alpha_1)(1 - t_s\alpha_0)]T_o + t_s\beta[(1 - t_s\alpha_1)u_0 + u_1] \\ &\quad + [(1 - t_s\alpha_1)t_s\gamma_0 + t_s\gamma_1], \\ T_3 &= [(1 - t_s\alpha_2)(1 - t_s\alpha_1)(1 - t_s\alpha_0)]T_o + t_s\beta[(1 - t_s\alpha_2)(1 - t_s\alpha_1)u_0 \\ &\quad + (1 - t_s\alpha_2)u_1 + u_2] \\ &\quad + [(1 - t_s\alpha_2)(1 - t_s\alpha_1)t_s\gamma_0 + (1 - t_s\alpha_2)t_s\gamma_1 + t_s\gamma_2], \\ &\vdots \\ T_{k+1} &= T_o\prod_{j=0}^{k}(1 - t_s\alpha_j) + t_s\beta\sum_{j=0}^{k}u_j\prod_{i=j+1}^{k}(1 - t_s\alpha_i) + \sum_{j=0}^{k}t_s\gamma_j\prod_{i=j+1}^{k}(1 - t_s\alpha_i), \end{aligned} \tag{18}$$

where T_o and T_k are the initial and k-th water temperatures inside the tank respectively. t_s is the sampling time, whereas u_k is the k-th switch status, which is either 1 or 0. α_j and γ_j are functions of Eqs. (8) and (10) respectively and β represents a constant given Eq. (9). The acceptable hot water temperature set points are given by inequality (19):

$$T_{low} \leqslant T_k \leqslant T_{up}, \tag{19}$$

where T_{low} and T_{up} are the lower and upper desired temperatures respectively.

3.2. Objective function

The objective function is the grid energy cost J minimization under the TOU tariff p_k in discrete time; the control variable is the grid power, $P_{g,k}$. The control horizon is one day, with t_s being the sampling time, and the sampling interval is $(1 \leqslant k \leqslant N)$.

The objective function:

$$J = t_s\sum_{k=1}^{N}P_{g,k}p_k, \tag{20}$$

subject to the following constraints:

$$\begin{aligned} T_{low} \leqslant\ & T_o\prod_{j=0}^{k}(1 - t_s\alpha_j) + t_s\beta\sum_{j=0}^{k}u_j\prod_{i=j+1}^{k}(1 - t_s\alpha_i) \\ & + \sum_{j=0}^{k}t_s\gamma_j\prod_{i=j+1}^{k}(1 - t_s\alpha_i) \leqslant T_{up}, \end{aligned} \tag{21}$$

$$P_{hp}u_k - P_{g,k} = P_{w,k} + P_{pv,k}, \tag{22}$$

$$0 \leqslant P_{pv,k} \leqslant P_{pv}^{max}, \tag{23}$$

$$0 \leqslant P_{w,k} \leqslant P_{w}^{rated}, \tag{24}$$

$$u_k \in \{0, 1\}, \tag{25}$$

where p_k is the TOU electricity tariff (R/kW h) at the k-th sampling interval. Inequality (21) shows the state variable (hot water temperature) at every sampling time k and lies between the lower and upper acceptable hot temperature set point. Whereas Eq. (22) represents the power balance, the summation of DREs and grid power is equal to the HPWH demand. The production of DREs continues even when the heat pump switch u_k is *off*(0); the excess power is fed into the grid. Inequality (23) and (24) are the power bounds of the PV and wind generator respectively. Eq. (25) is a binary switch control variable. At any given sampling interval its value is either 0 or 1, depicting the switch status of *off* or *on*.

[2] http://www.eskom.co.za/.
[3] http://www.nersa.org.za/.

3.3. Algorithm formulation

The proposed model has a binary variable and real number control variables, solved using the *OPTI toolbox* SCIP algorithm in MATLAB.

3.3.1. The objective function

The objective function is the total daily electrical energy cost under the TOU tariff given by,

$$f^T\mathbf{X} = [\,0 \quad \dots \quad 0_N, \quad p_1 \quad \dots \quad p_N\,] \begin{bmatrix} u_0 \\ \vdots \\ u_{N-1} \\ P_{g,0} \\ \vdots \\ P_{g,N-1} \end{bmatrix}_{2N\times 1}. \tag{26}$$

subject to

$$\begin{aligned} &\mathbf{AX} \leqslant \mathbf{b} \quad \text{(linear inequality constraint)},\\ &\mathbf{A_{eq}X} = \mathbf{b_{eq}} \quad \text{(linear equality constraint)}. \end{aligned} \tag{27}$$

The detailed optimization problem and constraints formulation is attached in Appendix A. The limits of the control variables are restricted between the lower and upper bounds, given in Eqs. (28) and (29).

lower bounds

$$lb^T = [\,0,\dots,0_N, \quad -\infty_1,\dots,-\infty_N\,], \tag{28}$$

upper bounds

$$ub^T = [\,1,\dots,1_N, \quad \infty_1,\dots,\infty_N\,]. \tag{29}$$

3.4. Case study

The case study is based on a farmhouse situated in the coastal town of Port Elizabeth in South Africa. The main intervention of this model proposes an optimal control and renewable power integration solution to the HPWH installed at this farmhouse. The current (baseline) situation is that the HPWH installed at the farmhouse is controlled by the digital thermostat and supplied by the grid alone. Despite this being the normal mode of control/-operation, it is far from optimal from a daily operational point of view.

Because of the operation constraints of the HPWH, the sampling time t_s is taken to be 30 min, giving the total sampling interval $N = 48$ per 24-h horizon. The 24-h daily simulation has been mentioned earlier in Section 1, because of several other factors such as lack of annual consolidated water demand and DREs output data in South Africa [41]. It is expected that the results of a day's performance may vary if modeled on an annual basis, because of variations in input data such wind power, PV power, and inlet water temperature over seasons. In this paper, a typical winter day is assumed because of its relatively higher hot water and energy demand, to simulate the worst case scenario. There are errors an a 24-h model's performance resulting from a variation of DREs and other input data over the season. However, these can be minimized by application of model predictive control in future research, as recommended in Section 5. Since cost minimization is the objective, for precise economic and payback (break-even) period estimation, simulations are done on each selected day in all seasons: summer, autumn, winter and spring in the case study. This increases the confidence level of the results with changing seasonal hot water demand, PV power generation, wind power generation and inlet cold water temperature variation that directly affect the annualised energy and cost savings calculated in subSection 4.6.

The average inlet cold water temperature,[4] T_{in}, in Port Elizabeth in early winter is shown in Fig. 2. The TOU electricity tariff color bar legend, off-peak (p_o), standard (p_s) and peak (p_p), in Fig. 2 applies to all associated figures in this paper.

The hot water demand flow rate $W_D(k)$ is shown in Fig. 3. According to the Department of Water Affairs and Forestry in South Africa, there is no consolidated database of information on household water consumption from water utilities [41]. It is only estimated to be around 50% of the total water demand used in domestic homes. Because of lack of accurate hot water demand data in the case study and at national level for this specific location, the average hot water demand survey conducted by Meyer [42,43] in selected cities of South Africa is adopted to validate this model's results.

The end-user at this farmhouse rarely uses hot water in the early and late hours of the day. June 3 is the sampled winter day in the case study; however, on this day there is no hot water usage between 00:00–05:00 and 22:00–00:00 mainly because the occupants are asleep during these periods. The preferred hot water temperature is set to $55\,^{\circ}\text{C} \leqslant T_k \leqslant 65\,^{\circ}\text{C}$; the average country ambient temperature of $T_a = 25\,^{\circ}\text{C}$ is used. The initial water temperature is set to $T_o = 60\,^{\circ}\text{C}$. However, the above desirable temperature varies from one individual to another.

3.4.1. Heat pump water heater parameters

The HPWH type is an air source tank-wrapped condenser coil, with the following parameters shown in Table 1.

3.4.2. Wind generator parameters

The wind generator in the case study is Ruam Energy[5] turbine with technical specifications given in Table 2. In this paper, η_t is the mechanical gearbox efficiency only. However, the overall wind-to-turbine power convention coefficient or the Betz limit C_p is factored in as well.

The wind turbine rated revolution per minute (RPM) is 280 RPM and a tower height to nacelle is approximately 16.6 m. The hourly wind speed at Port Elizabeth[6] and the consequent wind power generation, according to Eq. (12), are presented in Fig. 4.

3.4.3. Photovoltaic power generation

The PV power is input data in this model taken from our previous research [13,40].

In this model neither the PV nor the wind power generation is a control variable. Depending on the status of the HPWH, all DRE's power produced is fed into the grid during non-operational periods.

4. Simulation results and discussion

4.1. Optimal heat pump switching control strategy in winter

In Fig. 6 optimal control turns *on* the HPWH supply switch from 00:00 to 01:00 in the morning; thereafter, it keeps it turned *off* between 01:00 and 04:00. Thereafter, in order to avoid operating in peak TOU, the OC turns *on* after 04:00 to heat the water in advance to meet the anticipated hot water demand, which starts at 05:30, using the cheaper off-peak energy. It turns it *off* again towards 07:00, to avoid the standard TOU tariff so as to save energy cost. The HPWH is kept *off* till 16:00, when it turns *on* again

[4] http://www.wunderground.com/weather-forecast/ZA/Port_Elizabeth.html?MR=1.
[5] www.raumenergy.com.
[6] http://www.timeanddate.com/weather/south-africa/port-elizabeth/hourly.

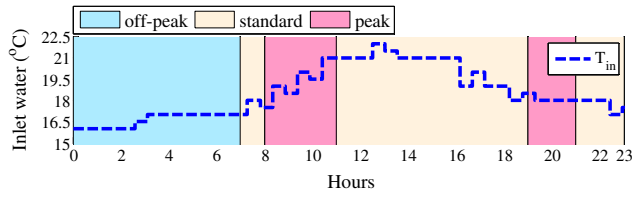

Fig. 2. Hourly inlet cold water temperature.

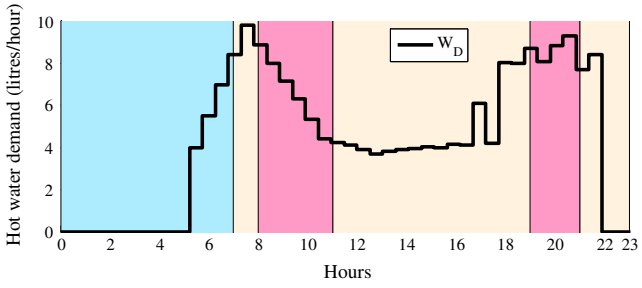

Fig. 3. Flow rate of hot water in winter.

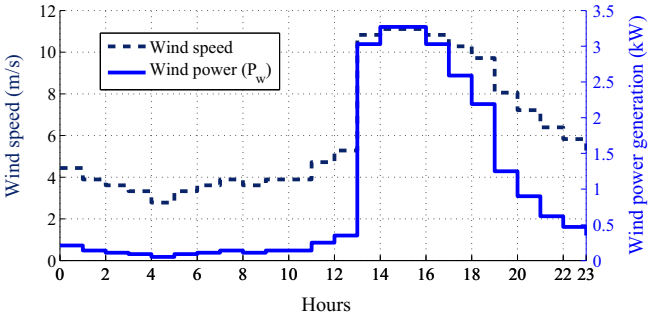

Fig. 4. Wind power output and speed for Port Elizabeth.

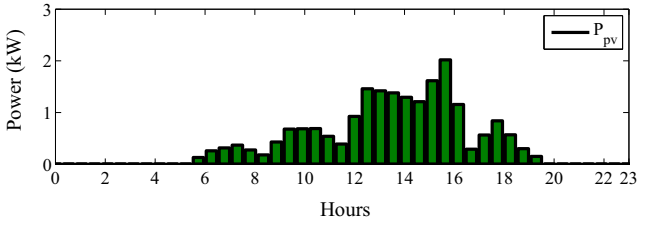

Fig. 5. Photovoltaic power output.

to preheat the water before the evening peak period, as a load-shifting strategy. Subsequently, after the evening peak it only comes *on* once again for 30 min to preheat the water. The OC finally turns *off* at 21:30 because at that time the hot water demand W_d declines to zero and the temperature is still above T_{low}, shown in Fig. 8.

The OC shows the ability to predict the demand and TOU accurately in order to save energy cost through load shifting, overcoming the limitation of a digital thermostat control strategy used in most HPWHs, as discussed in Section 4.3.

4.2. Optimal grid and feed-in power supply strategy in winter

The results of the OC power scheduling are presented in Fig. 7, showing wind power P_w, PV power P_{pv}, grid power P_g and HPWH P_{hp} demand. The grid power assumes negative values during feed-in and positive ones when supplying the HPWH load. In Fig. 7, P_g supplies the HPWH from midnight to 01:00, with very little supplement from wind power P_w. The slight deviation between HPWH demand P_{hp} and P_g is due to the low amount of power supplied by the wind generator. The grid stops supplying power between 01:00 and 04:00 because the HPWH is turned *off*, shown in Fig. 6, and begins accepting the little available wind power. At 04:00 the OC resumes grid supply till about 06:30 when the demand declines. PV power generation P_{pv} begins around the same time and the OC instantly resumes excess power feed-in into the grid.

From 07:00 the OC continues power feed-into the grid till 16:00. At 16:00, the OC stops feed-in; all the DREs' power is now used to meet the whole HPWH load turned *on*, though their combined power is unable to satisfy demand, prompting OC to bring in the grid P_g to supplement the deficit. OC is shown opting for cheaper renewable power whenever available to supply the HPWH as a mean of reducing energy cost. It manages to schedule load-shifting and avoid using peak TOU expensive energy, giving a cost benefit to the end-user.

4.3. Comparison between optimal and digital thermostat control strategies

Fig. 8 shows the hot water demand flow rate, a comparison of optimal and digital thermostat switching and finally the hot water temperature T_k. The OC switches *on* the HPWH from 00:00 to 01:00; the hot water temperature rises gradually from the initial $T_o = 60\,^{\circ}\text{C}$ to $61.5\,^{\circ}\text{C}$. Then temperature is observed to stay almost constant between 01:00 and 04:30, with a marginal decrease caused by convectional losses. Though the temperature in the above interval appears constant, it is merely because of the axis scaling; the half-hour temperature between 01:00 and 04:30

Table 1
Heat pump parameters.

Power input (kW)	COP	Storage capacity (l)	Compressor (cc)	Tank (h/ø) (m)	Δx (m)	κ (W/m K)	h (W/m^2 K)
6	3.8	270	39.0	1.41×0.66	0.035	0.055	6.3

Table 2
Wind generator parameters.

P_{wr} (kW)	η_t (%)	η_g (%)	ρ_a (kg/m^3)	C_p	A_w (m^2)	V_i (m/s)	V_N (m/s)	V_c (m/s)
3.5	0.9	0.8	1.22	0.48	11.3	3.2	11	50

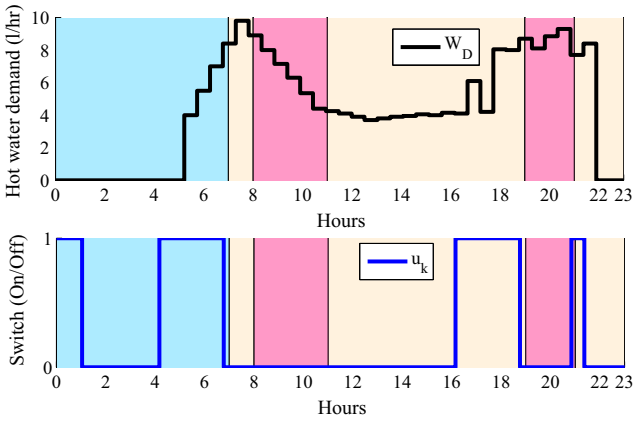

Fig. 6. Optimal heat pump power supply switching.

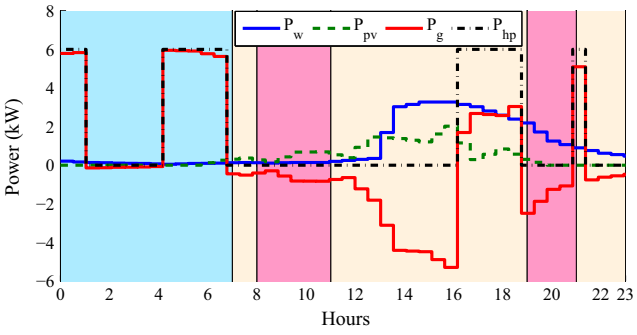

Fig. 7. Optimal grid and renewable power scheduling strategy.

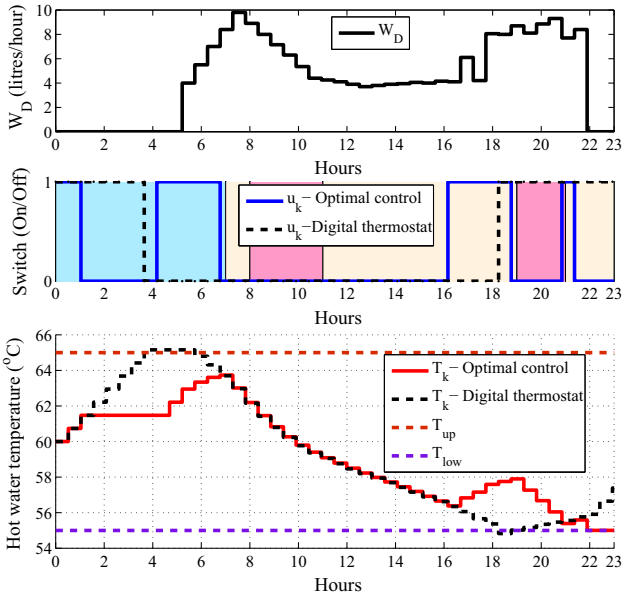

Fig. 8. Hot water temperature's dependency on switching and water usage.

shows a minimal temperature fall of 0.0008% due to the marginal standby losses. The limited hot water temperature drop in the absence of flow rate is owed to the good insulation of the HPWH tank in the case study.

Thereafter, the HPWH turns *on* again at 04:00, causing the water temperature to rise further. The non-linearity rise of T_k rise is due to the inlet of cold water into the tank as a result of hot water demand resumption. The temperature decrease after 07:00 is steady mainly because of the hot water consumption pattern. Since no water heating takes place from 07:00 to 16:00, the only major factors causing the decrease of T_k inlet of cold water and steady hot water demand usage. OC turns *on* the HPWH at 16:00 to preheat the water before evening peak TOU, effectively shifting the load. OC can predict the right time to turn *on* the HPWH so that the end-user is not inconvenienced and has hot water available at the right temperature.

The baseline situation is simulated as well to compare the benefits of OC over a digital thermostat control strategy which is used in most HPWHs on the market. The results of the comparison are also shown in Fig. 8. The digital thermostat (u_k – digital thermostat) turns *on* the HPWH from midnight till 03:30 and continues heating the water until T_k has reached the upper set point. It keeps it in operation regardless of whether there is hot water demand or not, using more energy. The hot water demand keeps decreasing T_k. By 18:00 it reaches the lower set point, hence the thermostat turns *on* again. Since it has no capability of load shifting, it runs throughout the peak period, incurring huge energy cost. In this study the switching *on* frequencies in the 24-h horizon are 13 and 20 times for the optimal and digital thermostat control strategy respectively. The OC has a lower switching frequency, which saves on energy and prolongs the compressor's life cycle.

However, it is worth pointing out that the desired temperature should not be set so high, beyond the rated capacity of the HPWH, as it will never reach that required temperature when demand for hot water occurs. A realistic temperature should be set within the range of the HPWH power rating, otherwise the end-user has to raise the water temperature inside the tank beforehand by some other means (e.g. by using an in-line resistive element heater).

4.4. Baseline and optimal energy savings in winter

Table 3 shows the daily energy and cost saving: baseline (digital thermostat control strategy) and optimal control strategy. The baseline energy is the current situation in the case study, where the 6 kW HPWH operates on the digital thermostat control strategy and is supplied by the grid alone, analogous. The baseline cost is the money paid for grid energy under the TOU electricity tariff prior to this proposed intervention. The optimal energy is the grid energy consumption after the implementation of this OC model integrated with DREs. The difference between the baseline energy and the optimal energy is what is referred to as the saved energy on the grid side, whereas, the optimal cost is the grid energy cost after intervention. In this model, the DREs' power consumed by the HPWH is assumed to be free energy, since after the initial investment cost the end-user uses this energy without paying for it. However, this energy is not necessarily free because of the invested resources. This is reflected in increased time to reach the break-even point in Section 4.6. The total feed-in energy, on

Table 3
Daily optimal energy savings.

Baseline (kW h/day)	Optimal (kW h/day)	Total feed-in (kW h/day)	Baseline cost (R/day)	Optimal cost (R/day)	Energy saving (%)	Cost saving (%)
60.00	29.26	23.24	48.83	14.29	51.23	70.74

the other hand, is the excess PV and wind energy fed into the utility grid when the HPWH is turned *off*.

The OC strategy yields 51.23% less energy consumption from the grid owing to a substantial supplement from wind and PV energy, which meets the HPWH load whenever available. The reduction of energy consumption from the grid consequently offers the power utility company positive climate mitigation and primary energy input relief that are not quantified in this paper. Hence, the proposed model is a near net-zero-energy building. A cost saving of 70.74% is realized, implying that this model has the potential to be cost-effective with the revenue from DREs sales.

The combined power output of DREs and the grid is shown in Fig. 9. The power flow of P_w and P_{pv} has been discussed earlier in Section 4.2. The baseline power $P_{g,baseline}$ supplies the HPWH from midnight till 04:00, meeting all the HPWH demand, since the grid is the only source of power. It is observed in the baseline scenario in Fig. 8 that the digital controller turns *on* the HPWH in the evening at 18:00 when the hot water temperature reaches the lower set point. The grid powers the HPWH throughout till 23:00 without consideration of the peak TOU, which is the major setback of this digital controller that reacts only to the state variable set point. On the contrary, the optimal control strategy is seen to schedule the grid power $P_{g,optimal}$ effectively to supplement DREs and avoids the peak periods. The load shifting strategy is to avoid expensive peak TOU electricity tariff, this effects a huge saving on energy cost. Here the OC shows the capability of load shifting, predicting and optimally keeping the hot water temperature within the desired set point using less energy to heat it to set points, while the digital thermostat controller clearly shows its limitation on T_k and load shifting.

Lastly, the feeding in of DREs' power occurs only when the HPWH turns *off*. The OC prioritizes the renewable power to supply the HPWH, only in cases where their combined power output is less than the demand. A marginal feed-in $P_{feed-in}$ of the available P_w power takes place from 01:30 to 04:00 owing to the absence of HPWH P_{hp} load. In the early morning at 06:30, the OC resumes the solar PV P_{pv} and wind P_w power feed-in into the main grid till 16:00. The optimal control stops the feed-in of power to the grid between 16:00 and 18:30 when the HPWH switches *on*; instead the grid $P_{g,optimal}$ is used to supplement the HPWH load deficit. Thereafter, the feed-in resumes till around 21:00 when it stops for a moment to aid the DRE. P_{pv} production ceases in these late hours of the day, so only wind energy is fed to the grid.

4.5. Effects of seasonal hot water demand variation on optimal temperature

The model is further simulated on a selected day in each of the four seasons to account for the varying hot water demand given in

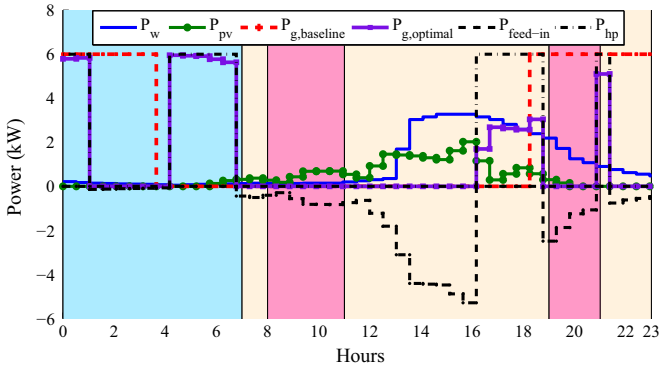

Fig. 9. Baseline and optimal power output.

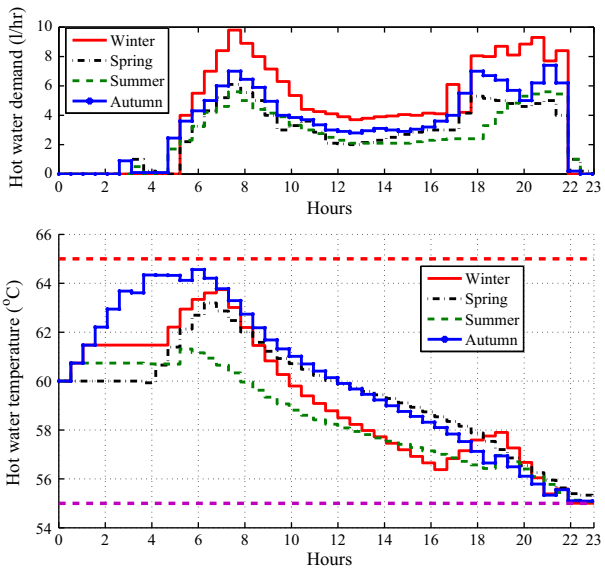

Fig. 10. Effects of seasonal hot water demand on optimal water temperature.

the case study, as shown in Fig. 10. The changing hot water demand shows an effect on the optimal energy and cost saving, because of the different scheduling strategy. Many factors affect the consumption of hot water, such as behavioral, and social ones, as well as ambient and inlet water temperatures. The simulation is run in each season to account for the consumption factor in order to determine the optimal cost and energy savings accurately. The savings, optimal benefit and sales of DREs sales are further averaged over the season and annualized for the calculation of the break-even period in Section 4.6.

The optimal hot water temperature is relatively similar in each season because of the similarity in the hot water usage in the house. In Fig. 10, autumn T_k steadily rises above other seasons because of the hot water consumption that starts earlier, around 02:30, making the OC turn *on* the HPWH before the demand for hot water starts. There is a reduction in the switching *on* frequency in the afternoons in most seasons owing to the improved inlet water temperature. However, in a typical situation, people still bath the same number of times regardless of the season, but; what reduces is the hot water requirement for mixing during a bath owing to the improved ambient temperatures.

4.5.1. Annualized feed-in energy and revenue

In order to estimate the reflective energy and revenue over a period of the year accurately, the simulation is run in each season on a selected day to account for demand variation and seasonal changes of wind and solar production, as well as inlet water temperature. The feed-in energy and revenue of each season are then averaged to reflect the day's value. The average value is annualized to reflect an average amount per annum. The energy cost saved

Table 4
Seasonal solar PV and wind generator feed-in.

Seasons	Winter	Spring	Summer	Autumn
Feed-in energy (kW h)				
Wind feed-in	15.08	22.72	21.58	20.80
Solar feed-in	8.17	10.01	9.79	9.79
Optimal grid energy	29.26	14.75	7.38	24.60
Revenue (R)				
Wind feed-in sales	18.84	28.40	26.97	25.99
Solar feed-in sales	32.17	39.42	38.55	38.55

Table 5
present value (PV).

Years	0	1	2	3	4	5
Initial capital investment						
Solar photovoltaic cost (R)	(27 500.00)					
Wind generator cost (R)	(23 500.00)					
Controllerscost (R)	(22 900.00)					
Inverters and accessories cost (R)	(15 000.00)					
Installation cost (R)	(14 000.00)					
Total investment cost (R)	(102 900.00)					
Maintenance and operation cost (R)		(2 500.00)	(2 500.00)	(2 500.00)	(2 500.00)	(2 500.00)
Expected annualised revenue						
Wind energy sales (R)		6 638.66	6 638.66	6 638.66	6 638.66	6 638.66
Solar energy sales (R)		13 568.47	13 568.47	13 568.47	13 568.47	13 568.47
Optimal benefit cost (R)		12607.10	12607.10	12607.10	12607.10	12607.10
Cash flows (CF)		30 314.24	30 314.24	30 314.24	30 314.24	30 314.24
Discount factor $(1+r)^{-n}$	1.00	0.96	0.92	0.88	0.84	0.81
Present value (PV)	(102 900.00)	29 036.63	27 812.86	26 640.67	25 517.88	24 442.42

after intervention is translated as a benefit cost or rather the amount the end-user would have spent had it not been for this intervention. The optimal benefit is the difference between baseline and optimal cost of a winter day, both in this simulation and in an annualized calculation. The HPWH operated for a total of 6.5 h in the case study. The switching *on/off* was dependent on the state variable, therefore the operation time varied on each day.

Table 4 shows the calculated seasonal energy and revenue. In order to calculate for example wind energy sales, a seasonal day's revenue is added $(R18.84 + R28.40 + R26.97 + R25.99)/4 = R25.05$ and averaged to determine a day's value over the year. Then this day value is multiplied by the number of days in a year $R25.05 \times 365 = R6638.66$/annum. This annualized revenue is then used to calculate the economic analysis of this proposed model. The averaging and simulation of a day in each season, increases the reliability of the proposed model and its financial feasibility, while at the same time meeting the technological and operational constraints of HPWH in the 24-h control horizon.

4.6. Economic analysis and payback period

In order to ascertain the economic viability of any project, investors and decision makers use the discounted payback period [44]. This approach firstly discounts the cash flows (CF) to determine a present value (PV) of money in the future. Then it establishes the period when the net present value (NPV) equal the total capital cost (CC) or the invested money which is when of break-even point (payback period) occurs. This is when the investor has recovered all his invested money. The initial capital investment in Table 4 is a negative cash flow in the financial statement (e.g., solar photovoltaic cost = $-R27500.00$) represented in brackets as (27500.00). The negative cash flows are the initial capital investment and all running cost of the project. Several assumptions are made when calculating the present value and payback period, the variation of inflation rate, depreciation, running and maintenance cost over time. However, for the purpose of present value and payback period calculation, the inflation rate, revenue and operational costs are assumed to be constant. Although it is expected that there would be an increase in all these factors, it cannot be reliably estimated at this time.

The payback period in this paper is obtained from the net present value (NPV) of the present value (PV). The present value of the cash flow during the n-th year, PV(n), formulated as [45]:

$$\mathrm{PV}(n) = \frac{\text{Cash flow}(n)}{(1+r)^n}, \tag{30}$$

Table 6
Discounted payback period.

Years	Present value	Net present value (PV)
0	(102900.00)	(102900.00)
1	29036.63	(73863.37)
2	27812.86	(46050.51)
3	**26640.67**	**(19409.84)**
4	25517.88	6108.04
5	24442.42	30550.46

where cash flow(n) denotes the cash flow of the n-th year and r denotes the discount rate. The formula of the cash flow is project specific and the tabulation of the results are shown in Table 4.

Table 5 shows the revenue from solar energy sales, wind energy sales and OC benefit. The cash flows and pay back-period is calculated making the assumptions that the solar sales, wind sales, cost saving, operational and maintenance costs will remain constant throughout the period. A discount factor or interest rate of 4.4% for February 2015 in the case study is used to reflect the time value of money. The 4.4% is indicative of the inflation rate in South Africa. The prices[7] of most components are based on the local product supplier and all amounts are in South African rand, while the wind generator and PV size are shown in Table 2 and Section 3.4.3 respectively.

Usually, for most of energy-efficiency project economic analysis, the operating cost, maintenance cost and cost savings are taken into account. Having obtained PV(n), the net present value is:

$$\mathrm{NPV}_{n=1}^{m} = \sum_{n=1}^{m} \mathrm{PV}(n) - \mathrm{CC}, \tag{31}$$

where CC is the initial capital cost of the project. Thereafter, the discounted payback period is obtained as

$$\text{Payback period} = m_y + \frac{-\mathrm{NPV}_{n=1}^{m}}{\mathrm{PV}(m_y+1)}, \tag{32}$$

where m_y denotes the last year with a negative NPV and the results are presented in Table 6.

The NPV continues to decrease in negative cash flow till a point when it crosses to positive cash flows. The payback/break-even happens at the point when the cumulative cash flow equals zero. This is the point at which all the invested capital is recovered. Thereafter, NPV goes into positive values, meaning the whole capital cost has been fully recovered, all the revenue in subsequent years to follow

[7] www.dako.co.za.

is pure profit; though maintenance cost is expected to be high owing to ageing equipment, it is not considered in this paper.

According to Table 6, the pay-back period is 3 years and 9 months, the break-even year is highlighted in bold. The break-even period is shorter owing to the optimal benefits. The money generated from the feed-in sales can still assist to offset the power utility bills. Therefore, this optimal switching control is beneficial for those intending to transform their homes into cost-effective and net-zero energy buildings in countries with an attractive feed-in tariff.

5. Conclusions

The TOU based optimal switching control shows the potential to save energy cost, as well as energy-not-delivered on the utility side, thus a reduction on primary inputs and greenhouse gases. This model yields a maximum energy saving of 51.23% and has the potential to be cost-effective on energy bills. This intervention provides a practical optimal integration of wind and other DREs into homes, with the benefit of energy trade-off and the possibility of achieving a net zero-energy building.

The economic analysis shows a payback period of 3 years and 9 months. There are other incentives pertaining to rebates on HPWH, wind power and solar PV application that are not considered in this paper, which are evident in the case study and could further reduce the payback period.

This model is suitable for application in both peri-urban and rural areas, in the generation of hot water, space heating and renewable energy integration. However, there is a need for future research into the application of model predictive control with feedback to minimize disturbances arising from wind and PV variations and hot water demand. There is a need as well to incorporate other renewable sources, such as biomass and fuel cells to supply energy-efficient household equipment. It can be adopted by home-owners who want to integrate renewable energy sources using energy-efficient equipment such as HPWH to save energy with the minimum environmental impact. The OC strategy offers the potential to be cost-effective and to overcome the limitations of digital thermostat control used in most heat pumps on the market.

Acknowledgements

The authors would like to thank the National Research Foundation (NRF) of South Africa grant NRF SFH14080687344, Maastricht University under NUFFIC – MUNDO Project No: NICHE ZMB 037 Netherlands, The University of Zambia and the National Hub for Energy Efficiency and Demand Side Management (EEDSM) for financial and other support for this research.

Appendix A. Algorithm formulation

The proposed model has a binary variable and real number control variables, solved using the *OPTI toolbox* SCIP algorithm in MATLAB.

A.1. Inequality matrices

The general formulation of the inequality constraint is shown in Eq. (A.1):

$$\mathbf{AX} \leqslant \mathbf{b}. \tag{A.1}$$

Vector $\mathbf{X}$ comprises all the control variables: switch u_k and grid power P_g written in Eq. (A.3). Let matrix $\mathbf{A}$ and vector $\mathbf{b}$ be:

$$\mathbf{A} = \begin{bmatrix} \mathbf{A_1} \\ -\mathbf{A_1} \end{bmatrix}, \quad \mathbf{b} = \begin{bmatrix} \mathbf{b_1} \\ \mathbf{b_2} \end{bmatrix}, \tag{A.2}$$

and,

$$\mathbf{X} = \begin{bmatrix} u_0 \\ \vdots \\ u_{N-1} \\ P_{g,0} \\ \vdots \\ P_{g,N-1} \end{bmatrix}_{2N\times 1}. \tag{A.3}$$

Then matrix $\mathbf{A_1}$ is an $N \times 2N$ matrix given in Eq. (A.4):

$$\mathbf{A_1} = t_s\beta \begin{bmatrix} 1 & 0 & 0 & 0 & \dots & 0 & 0 & \dots & 0 \\ (1-t_s\alpha_1) & 1 & 0 & 0 & \dots & 0 & 0 & \dots & 0 \\ (1-t_s\alpha_2)(1-t_s\alpha_1) & (1-t_s\alpha_2) & 1 & 0 & \dots & 0 & 0 & \dots & 0 \\ \vdots & \vdots & \vdots & \ddots & \vdots & \vdots & 0 & \dots & 0 \\ (1-t_s\alpha_{N-2})\times\dots\times(1-t_s\alpha_1) & (1-t_s\alpha_{N-2})\times\dots\times(1-t_s\alpha_2) & \dots & \dots & 1 & 0 & 0 & \dots & 0 \\ (1-t_s\alpha_{N-1})(1-t_s\alpha_{N-2})\times\dots\times(1-t_s\alpha_1) & (1-t_s\alpha_{N-1})\times\dots\times(1-t_s\alpha_2) & \dots & \dots & (1-t_s\alpha_{N-1}) & 1 & 0 & \dots & 0 \end{bmatrix}, \tag{A.4}$$

inequality (21) is reformulated into inequality (A.5) and inequality (A.6):

$$t_s\beta\sum_{j=0}^{k} u_j \prod_{i=j+1}^{k}(1-t_s\alpha_i) \leqslant T_{up} - T_o\prod_{j=0}^{k}(1-t_s\alpha_j) - \sum_{j=0}^{k} t_s\gamma_j \prod_{i=j+1}^{k}(1-t_s\alpha_i), \tag{A.5}$$

$$-t_s\beta\sum_{j=0}^{k} u_j \prod_{i=j+1}^{k}(1-t_s\alpha_i) \leqslant -T_{low} + T_o\prod_{j=0}^{k}(1-t_s\alpha_j) + \sum_{j=0}^{k} t_s\gamma_j \prod_{i=j+1}^{k}(1-t_s\alpha_i). \tag{A.6}$$

According to inequality (A.5) and inequality (A.6), the element of vectors $\mathbf{b_1}$ and $\mathbf{b_2}$ is:

$$b_{1,k} = T_{up} - T_o\prod_{j=0}^{k}(1-t_s\alpha_j) - \sum_{j=0}^{k} t_s\gamma_j \prod_{i=j+1}^{k}(1-t_s\alpha_i), \tag{A.7}$$

$$b_{2,k} = -T_{low} + T_o\prod_{j=0}^{k}(1-t_s\alpha_j) + \sum_{j=0}^{k} t_s\gamma_j \prod_{i=j+1}^{k}(1-t_s\alpha_i). \tag{A.8}$$

Vector $\mathbf{b_1}$ in Eq. (A.7) is the difference in three vectors $\mathbf{b_3}$, $\mathbf{b_4}$ and $\mathbf{b_5}$, as shown in Eq. (A.9).

$$\mathbf{b_1} = \mathbf{b_3} - \mathbf{b_4} - \mathbf{b_5}, \tag{A.9}$$

where

$$\mathbf{b_3} = \begin{bmatrix} T_{up} \\ \vdots \\ T_{up} \end{bmatrix}_{N\times 1}, \tag{A.10}$$

then vector $\mathbf{b_4}$ is given in Eq. (A.11),

$$\mathbf{b_4} = T_o \begin{bmatrix} (1-t_s\alpha_0) \\ (1-t_s\alpha_1)(1-t_s\alpha_0) \\ (1-t_s\alpha_2)(1-t_s\alpha_1)(1-t_s\alpha_0) \\ \vdots \\ (1-t_s\alpha_{N-2})(1-t_s\alpha_{N-3})\times\cdots\times(1-t_s\alpha_0) \\ (1-t_s\alpha_{N-1})(1-t_s\alpha_{N-2})(1-t_s\alpha_{N-3})\times\cdots\times(1-t_s\alpha_0) \end{bmatrix}_{N\times 1}, \tag{A.11}$$

and finally, $\mathbf{b_5}$ is given in Eq. (A.12) below,

$$\mathbf{b_5} = \begin{bmatrix} t_s\gamma_o \\ (1-t_s\alpha_1)t_s\gamma_o + t_s\gamma_1 \\ (1-t_s\alpha_2)(1-t_s\alpha_1)t_s\gamma_o + (1-t_s\alpha_2)t_s\gamma_1 + t_s\gamma_2 \\ \vdots \\ (1-t_s\alpha_{N-2})\times\cdots\times(1-t_s\alpha_1)t_s\gamma_o + (1-t_s\alpha_{N-2})\times\cdots\times(1-t_s\alpha_2)t_s\gamma_1 + \cdots + t_s\gamma_{N-2} \\ (1-t_s\alpha_{N-1})(1-t_s\alpha_{N-2})\times\cdots\times(1-t_s\alpha_1)t_s\gamma_o + (1-t_s\alpha_{N-1})\times\cdots\times(1-t_s\alpha_2)t_s\gamma_1 + \cdots (1-t_s\alpha_{N-1})t_s\gamma_{N-2} + t_s\gamma_{N-1} \end{bmatrix}. \tag{A.12}$$

The T_{low} vector is given in Eq. (A.13), the formulation of the $\mathbf{b_2}$ vector is analogous to $\mathbf{b_1}$ given in Eq. (A.14),

$$\mathbf{b_6} = \begin{bmatrix} T_{low} \\ \vdots \\ T_{low} \end{bmatrix}_{N\times 1}, \tag{A.13}$$

$$\mathbf{b_2} = -\mathbf{b_6} + \mathbf{b_4} + \mathbf{b_5}. \tag{A.14}$$

A.2. Equality matrices

The power balance Eq. (16) constitutes an equality constraint, a sparse matrix $\mathbf{A_{eq}}$, given in Eq. (A.15):

$$\mathbf{A_{eq}} = \begin{bmatrix} P_{hp} & 0 & \cdots & 0 & \vdots & -1 & 0 & \cdots & 0 \\ 0 & P_{hp} & 0 & \cdots & \vdots & 0 & \ddots & \cdots & 0 \\ \vdots & 0 & \ddots & 0 & \vdots & \vdots & 0 & -1 & \vdots \\ 0 & 0 & \cdots & P_{hp} & \vdots & 0 & 0 & \cdots & -1 \end{bmatrix}_{N\times 2N}. \tag{A.15}$$

The k-th total PV and wind power constituting of element of vector $\mathbf{b_{eq}}$ is shown in Eq. (A.16):

$$\mathbf{b_{eq}} = \begin{bmatrix} P_{w,1} + P_{pv,1} \\ \vdots \\ P_{w,N} + P_{pv,N} \end{bmatrix}_{N\times 1}. \tag{A.16}$$

Therefore, the canonical form is $\mathbf{A_{eq}X} = \mathbf{b_{eq}}$ where $\mathbf{A_{eq}}$ is given in Eq. (A.15) and $\mathbf{b_{eq}}$ in Eq. (A.16).

A.3. The objective function

The objective function is the total daily electrical energy cost under the TOU tariff given by,

$$f^T\mathbf{X} = [\,0 \quad \ldots \quad 0_N, \quad p_1 \quad \ldots \quad p_N\,] \begin{bmatrix} u_0 \\ \vdots \\ u_{N-1} \\ P_{g,0} \\ \vdots \\ P_{q,N-1} \end{bmatrix}_{2N\times 1}. \tag{A.17}$$

The limits of the control variables are restricted between the lower and upper bounds, given in Eqs. (A.18) and (A.19).

lower bounds

$$lb^T = [\,0 \quad \ldots \quad 0_N, \quad -\infty_1 \quad \ldots \quad -\infty_N\,], \tag{A.18}$$

upper bounds

$$ub^T = [\,1 \quad \ldots \quad 1_N, \quad \infty_1 \quad \ldots \quad \infty_N\,]. \tag{A.19}$$

References

[1] Rahman MM, Rasul M, Khan MMK. Energy conservation measures in an institutional building in sub-tropical climate in Australia. Appl Energy 2010;87(10):2994–3004.

[2] Esen H, Inalli M, Esen M. Technoeconomic appraisal of a ground source heat pump system for a heating season in eastern Turkey. Energy Convers Manage 2006;47(10):1281–97.

[3] Chua K, Chou S, Yang W. Advances in heat pump systems: a review. Appl Energy 2010;87(12):3611–24.

[4] Chow T, Bai Y, Fong K, Lin Z. Analysis of a solar assisted heat pump system for indoor swimming pool water and space heating. Appl Energy 2012;100:309–17.

[5] Esen M, Yuksel T. Experimental evaluation of using various renewable energy sources for heating a greenhouse. Energy Buildings 2013;65(0):340–51.

[6] Roonprasang N, Namprakai P, Pratinthong N. Experimental studies of a new solar water heater system using a solar water pump. Energy 2008;33(4):639–46.

[7] Tamasauskas J, Poirier M, Zmeureanu R, Sunyé R. Modeling and optimization of a solar assisted heat pump using ice slurry as a latent storage material. Sol Energy 2012;86(11):3316–25.

[8] Zhang X, Zhao X, Xu J, Yu X. Characterization of a solar photovoltaic/loop-heat-pipe heat pump water heating system. Appl Energy 2013;102:1229–45.

[9] Ji J, Pei G, Chow T-t, He W, Zhang A, Dong J, et al. Performance of multi-functional domestic heat-pump system. Appl Energy 2005;80(3):307–26.

[10] Lane I, Beute N. A model of the domestic hot water load. IEEE Trans Power Syst 1996;11(4):1850–5.

[11] Tian Y, Zhao C-Y. A review of solar collectors and thermal energy storage in solar thermal applications. Appl Energy 2013;104:538–53.
[12] Rankin R, Rousseau PG, van Eldik M. Demand side management for commercial buildings using an inline heat pump water heating methodology. Energy Convers Manage 2004;45(9):1553–63.
[13] Sichilalu SM, Xia X. Optimal energy control of grid tied PV–diesel–battery hybrid system powering heat pump water heater. Sol Energy 2015;115:243–54.
[14] Mellit A, Benghanem M, Kalogirou S. Modeling and simulation of a stand-alone photovoltaic system using an adaptive artificial neural network: proposition for a new sizing procedure. Renew Energy 2007;32(2):285–313.
[15] Kellogg W, Nehrir M, Venkataramanan G, Gerez V. Optimal unit sizing for a hybrid wind/photovoltaic generating system. Electric Power Syst Res 1996;39 (1):35–8.
[16] Khatib T, Mohamed A, Sopian K. Optimization of a PV/wind micro-grid for rural housing electrification using a hybrid iterative/genetic algorithm: case study of Kuala Terengganu, Malaysia. Energy Buildings 2012;47:321–31.
[17] Nayar C, Phillips S, James W, Pryor T, Remmer D. Novel wind/diesel/battery hybrid energy system. Sol Energy 1993;51(1):65–78.
[18] Mathaba T, Mpholo M, Letuma M. Velocity and power density analysis of the wind at letšeng-la-terae in Lesotho. Renew Energy 2012;46:210–7.
[19] Moghavvemi M, Ismail M, Murali B, Yang S, Attaran A, Moghavvemi S. Development and optimization of a PV/diesel hybrid supply system for remote controlled commercial large scale fm transmitters. Energy Convers Manage 2013;75:542–51.
[20] Zhao Y, Lu Y, Yan C, Wang S. MPC-based optimal scheduling of grid-connected low energy buildings with thermal energy storages. Energy Buildings 2015;86: 415–26.
[21] Zeiler W, Boxem G. Net-zero energy building schools. Renew Energy 2013;49 (0):282–6.
[22] Torcellini PA, Crawley DB. Understanding zero-energy buildings. ASHRAE J 2006;48(9):62–9.
[23] Bengea SC, Decarlo RA. Optimal control of switching systems. Automatica 2005;41(1):11–27.
[24] Sichilalu S, Xia X, Zhang J. Optimal scheduling strategy for a grid-connected photovoltaic system for heat pump water heaters. Energy Procedia 2014;61: 1511–4.
[25] Sichilalu SM, Xia X. Optimal power dispatch of a grid tied-battery-photovoltaic system supplying heat pump water heaters. Energy Convers Manage 2015; 102:81–91.
[26] Sun X, Dai Y, Novakovic V, Wu J, Wang R. Performance comparison of direct expansion solar-assisted heat pump and conventional air source heat pump for domestic hot water. Energy Procedia 2015;70(0):394–401.
[27] Mehrpooya M, Hemmatabady H, Ahmadi MH. Optimization of performance of combined solar collector-geothermal heat pump systems to supply thermal load needed for heating greenhouses. Energy Convers Manage 2015;97(0): 382–92.
[28] Kusakana K. Operation cost minimization of photovoltaic–diesel–battery hybrid systems. Energy 2015;85:645–53.
[29] Fraga C, Mermoud F, Hollmuller P, Pampaloni E, Lachal B. Large solar driven heat pump system for a multifamily building: long term in-situ monitoring. Sol Energy 2015;114(0):427–39.
[30] Verhelst C, Degrauwe D, Logist F, Van Impe J, Helsen L. Multi-objective optimal control of an air-to-water heat pump for residential heating. Build Simul 2012;5(3):281–91.
[31] Paull L, Li H, Chang L. A novel domestic electric water heater model for a multi-objective demand side management program. Electric Power Syst Res 2010;80 (12):1446–51.
[32] Ranaboldo M, Domenech B, Reyes GA, Ferrer-Martí L, Moreno RP, García-Villoria A. Off-grid community electrification projects based on wind and solar energies: a case study in Nicaragua. Sol Energy 2015;117:268–81.
[33] Kim M, Kim MS, Chung JD. Transient thermal behavior of a water heater system driven by a heat pump. Int J Refrig 2004;27(4):415–21.
[34] Zhang J, Xia X. Best switching time of hot water cylinder-switched optimal control approach. In: AFRICON 2007. IEEE; 2007. p. 1–7.
[35] Khan K, Rasul M, Khan MMK. Energy conservation in buildings: cogeneration and cogeneration coupled with thermal energy storage. Appl Energy 2004;77 (1):15–34.
[36] Gustafson M, Baylor J, Epstein G. Direct water heater load control-estimating program effectiveness using an engineering model. IEEE Trans Power Syst 1993;8(1):137–43.
[37] Dolan P, Nehrir M, Gerez V. Development of a monte carlo based aggregate model for residential electric water heater loads. Electric Power Syst Res 1996;36(1):29–35.
[38] Ashok S. Optimised model for community-based hybrid energy system. Renew Energy 2007;32(7):1155–64.
[39] Li H, Chen Z, Polinder H. Optimization of multibrid permanent-magnet wind generator systems. IEEE Trans Energy Convers 2009;24(1):82–92.
[40] Tazvinga H, Xia X, Zhang J. Minimum cost solution of photovoltaics–diesel–battery hybrid power systems for remote consumers. Sol Energy 2013;96: 292–9.
[41] Department of Water Affairs and Forestry, South Africa. Water conservation and demand management strategy for the water services sectors; August 2004.
[42] Meyer JP. A review of domestic hot-water consumption in South Africa. R&D J 2000;16:p55–61.
[43] Meyer J, Tshimankinda M. Domestic hot water consumption in South African townhouses. Energy Convers Manage 1998;39(7):679–84.
[44] Jaffe J, Randolph Westerfield R, et al. Corporate finance. Tata McGraw-Hill Education; 2005.
[45] Fabrycky WJ, Blanchard BS. Life-cycle cost and economic analysis. Prentice Hall; 1991.